Cytoskeleton assembly at endothelial cell–cell contacts is regulated by αII-spectrin–VASP complexes

Peter M. Benz,[1] Constanze Blume,[1] Jan Moebius,[2] Chris Oschatz,[1] Kai Schuh,[1] Albert Sickmann,[2] Ulrich Walter,[1] Stephan M. Feller,[3] and Thomas Renné[1]

[1]Institute of Clinical Biochemistry and Pathobiochemistry and [2]Rudolf-Virchow-Center for Experimental Biomedicine, University of Würzburg, D-97080 Würzburg, Germany
[3]Cell Signalling Group, Weatherall Institute of Molecular Medicine, John Radcliffe Hospital, Oxford OX3 9DS, England, UK

Directed cortical actin assembly is the driving force for intercellular adhesion. Regulated by phosphorylation, vasodilator-stimulated phosphoprotein (VASP) participates in actin fiber formation. We screened for endothelial proteins, which bind to VASP, dependent on its phosphorylation status. Differential proteomics identified αII-spectrin as such a VASP-interacting protein. αII-Spectrin binds to the VASP triple GP_5-motif via its SH3 domain. cAMP-dependent protein kinase–mediated VASP phosphorylation at Ser157 inhibits αII-spectrin–VASP binding. VASP is dephosphorylated upon formation of cell–cell contacts and in confluent, but not in sparse cells, αII-spectrin colocalizes with nonphosphorylated VASP at cell–cell junctions. Ectopic expression of the αII-spectrin SH3 domain at cell–cell contacts translocates VASP, initiates cortical actin cytoskeleton formation, stabilizes cell–cell contacts, and decreases endothelial permeability. Conversely, the permeability of VASP-deficient endothelial cells (ECs) and microvessels of VASP-null mice increases. Reconstitution of VASP-deficient ECs rescues barrier function, whereas αII-spectrin binding-deficient VASP mutants fail to restore elevated permeability. We propose that αII-spectrin–VASP complexes regulate cortical actin cytoskeleton assembly with implications for vascular permeability.

Introduction

Endothelial cells (ECs) line vessel walls and control the transition of water and plasma proteins between blood and the underlying tissue. Endothelial barrier function depends on interendothelial junctions (IEJs), and defective sealing of cell–cell contacts increases paracellular leakage that may result in edema formation (Dejana, 2004). Control of perijunctional actin assembly appears to be the unifying mechanism for regulating endothelial junctions and paracellular permeability (Mitic and Anderson, 1998; Mehta and Malik, 2006).

Members of the Enabled/vasodilator-stimulated phosphoprotein (Ena/VASP) protein family are involved in cortical actin dynamics, although their exact function for cytoskeletal regulation remains unclear (Vasioukhin et al., 2000; Scott et al., 2006). In mammals, the Ena/VASP family consists of the following three proteins: mammalian Ena (Mena), VASP, and Ena-VASP–like (EVL). The family members share a tripartite domain organization of an N-terminal Ena/VASP homology 1 (EVH1) domain, a central proline-rich region (PRR), and an EVH2 domain at the C terminus (Kwiatkowski et al., 2003; Sechi and Wehland, 2004). The EVH1 domain mediates binding of Ena/VASP proteins to proline-rich ligands such as vinculin and zyxin (Ball et al., 2000). The PRR interacts with the actin-binding protein profilin and with Src homology 3 (SH3) domains (Lambrechts et al., 2000; Howe et al., 2002), whereas the EVH2 domain mediates tetramerization and actin binding (Bachmann et al., 1999; Kuhnel et al., 2004). VASP harbors three serine/threonine phosphorylation sites. S157 is located N-terminally of the central PRR. S239 and T278 are within the EVH2 domain, adjacent to the G- and F-actin binding sites, respectively (Kwiatkowski et al., 2003). In vivo, S157 is preferentially phosphorylated by the cAMP-dependent protein kinase (PKA), whereas S239 and T278 are targeted by the cGMP-dependent protein kinase (PKG) or the AMP-activated protein kinase (AMPK), respectively (Blume et al., 2007). Phosphorylation of VASP regulates its affinity for F-actin (Lambrechts et al., 2000; Barzik et al., 2005) and SH3 domains (Howe et al., 2002).

Correspondence to Thomas Renné: thomas@renne.net

Abbreviations: AMPK, AMP-activated protein kinase; EC, endothelial cell; EVH, Ena/VASP homology; EVL, Ena-VASP–like; IEJ, interendothelial junction; MALDI-TOF, matrix-assisted laser desorption ionization time-of-flight; PMF, peptide mass fingerprinting; PRR, proline-rich region; VASP, vasodilator-stimulated phosphoprotein.

The online version of this article contains supplemental material.

The Journal of Cell Biology, Vol. 180, No. 1, January 14, 2008 205–219
http://www.jcb.org/cgi/doi/10.1083/jcb.200709181

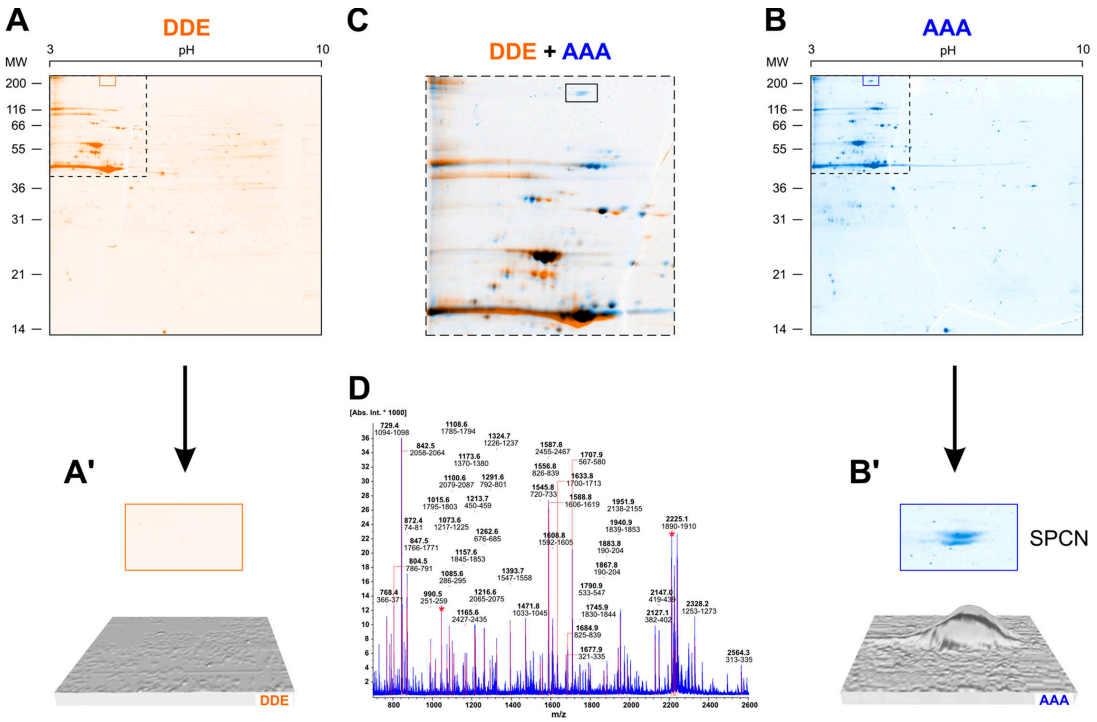

Figure 1. **αII-Spectrin (SPCN) is a new VASP-binding protein in ECs.** Proteins that bind to VASP dependent on its phosphorylation status were isolated from EA.hy926 cell cytosol by affinity chromatography columns with coupled VASP-DDE (orange) or -AAA (blue). Eluted proteins were separated by 2D-PAGE and stained with colloidal Coomassie (A and B). (C) Merged and magnified image of areas indicated by dashed boxes in A and B. Black spots represent proteins that bind to both VASP forms. The boxed spot marks αII-spectrin (SPCN). (A′ and B′) Magnification of the SPCN spot in B and the corresponding gel area in A (top), and 3D densitograms of the signal intensities (bottom). (D) MALDI-PMF spectrum of the spot in B′ identified SPCN. Annotated peaks represent identified peptides, which are labeled with the exact mass (bold letters) and the amino acid positions of the protein. Peaks marked with asterisks represent trypsin-fragments, which originate from autodigestion of the protease.

Originally identified in erythrocytes, spectrins are evolutionary conserved rod-shaped proteins that associate with actin filaments to form a 2D meshwork at the cytoplasmic face of the plasma membrane. Spectrins exist as heterotetramers $(\alpha, \beta)_2$, composed of α and β subunits, which show distinct functions and tissue-specific expression (Bennett and Baines, 2001). The αII-spectrin subunit (also known as SPCN, α-fodrin, and nonerythroid α-spectrin) is ubiquitously expressed (except erythrocytes) and predominantly exists as αII/βII tetramers (Heltianu et al., 1986). Spectrins are scaffolders and assemble a multifunctional interface that links membranes to filaments of the perijunctional cytoskeleton (De Matteis and Morrow, 2000). Spectrins cluster transmembrane adhesion proteins within plasma membrane microdomains and couple them to the spectrin–actin network on both sites of the junction (De Matteis and Morrow, 2000; Pinder and Baines, 2000).

In this study, we identified αII-spectrin as a new VASP-binding protein and characterized structure, regulation, and function of αII-spectrin interaction with VASP with importance for endothelial cell–cell adhesion and vascular permeability.

Results

αII-Spectrin (SPCN) is a new VASP-binding protein in ECs

VASP is phosphorylated by PKA, PKG, and AMPK at residues S157, S239, and T278, respectively. We used differential proteomics to identify endothelial proteins that bind to VASP dependent on its phosphorylation status. VASP pseudophosphorylation mutants VASP-DDE and -AAA (which mimic completely phosphorylated or unphosphorylated protein, respectively) were expressed in *Escherichia coli*, purified, and linked to an affinity chromatography matrix. Cytosolic proteins from confluent EA.hy926 ECs were applied to columns with immobilized VASP mutants. Specifically bound proteins were eluted by a pH gradient. We probed the eluates for known VASP-interacting proteins and detected zyxin and vinculin in the pH 2.0 fraction by Western blotting. Proteins of this fraction were analyzed using 2D-PAGE. Colloidal Coomassie blue staining detected >100 VASP-binding proteins in the eluates of VASP-DDE and -AAA columns, respectively (representative 2D gels from $n = 6$; Fig. 1, compare A, B, and the merged image C). A protein spot with apparent molecular weight of >200 kD was eluted from VASP-AAA, but not from VASP-DDE (Fig. 1, A' and B'). Using matrix-assisted laser desorption ionization time-of-flight (MALDI-TOF) peptide mass fingerprinting (PMF), we identified the protein as αII-spectrin (SPCN; mascot score of 257; National Center for Biotechnology Information sequence identification number gil31565122; Fig. 1 D). The calculated pI of 5.2 and molecular weight of 240 kD of SPCN is consistent with the observed migration behavior in the 2D gel.

VASP interacts with SPCN at sites of interendothelial adhesion

To confirm the interaction of SPCN and VASP, confluent EA.hy926 cells were lysed, immunoprecipitated with antibodies against

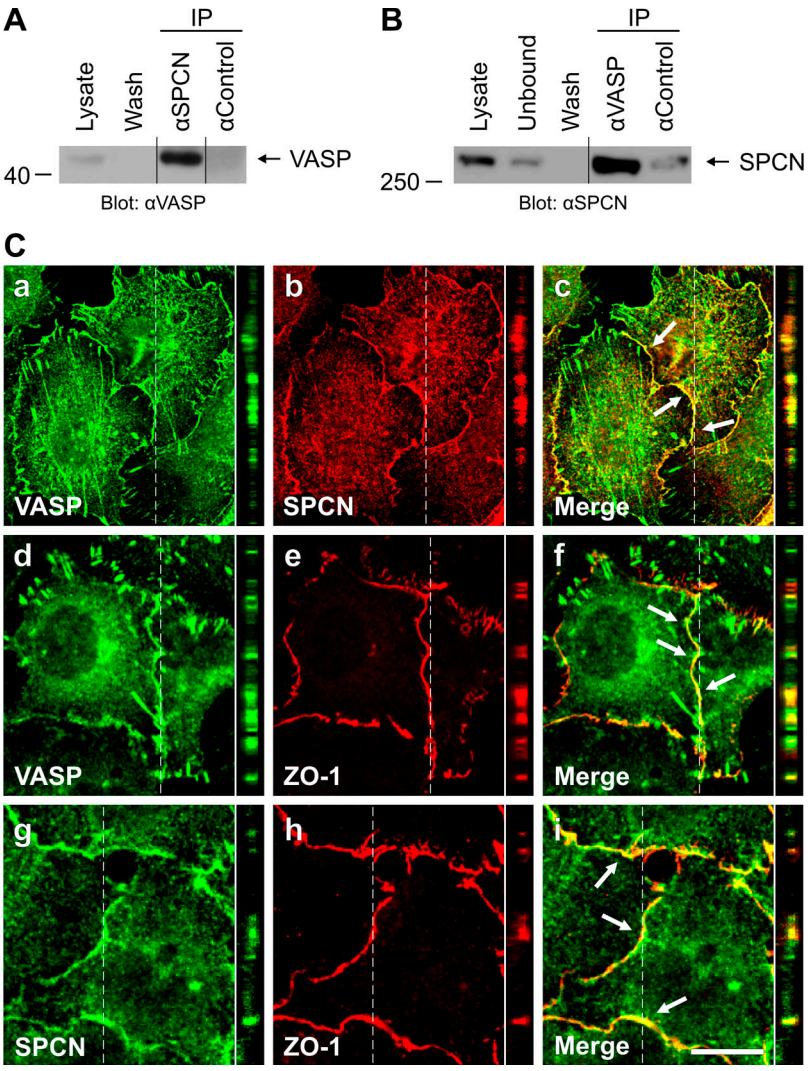

Figure 2. **VASP interacts with SPCN at sites of inter-endothelial adhesion.** (A and B) Lysates of confluent EA.hy926 cells were immunoprecipitated (IP) with antibodies against SPCN, VASP, or unrelated proteins (Control). Lysate, wash fraction (Wash), and precipitated material were analyzed by Western blot with anti-VASP (A) or -SPCN (B) antibodies. Cell lysate immunodepleted by anti-VASP antibodies and blotted for SPCN is shown in (B, Unbound). (C) Confocal immunofluorescence images of fixed and permeabilized ECV304 cells. Cells were stained for VASP (a and d), SPCN (b and g), and ZO-1 (e and h). Yellow color indicates colocalized VASP and SPCN (c), VASP and ZO-1 (f), and SPCN and ZO-1 (i). Insets on the right are confocal sections in the vertical plane of the Z-stacks, taken at the position of the dashed line. Arrows indicate sites of colocalization. Bar, 15 μm.

VASP, and precipitated material was probed with anti-SPCN antibodies or vice versa. Western blots indicated that SPCN and VASP mutually and specifically immunoprecipitated each other (Fig. 2, A and B). Comparison of SPCN signal intensities in lysed cells and in immunodepleted lysate indicated that >70% of cellular SPCN was coprecipitated by VASP (Fig. 2 B, compare Lysate and Unbound), suggesting that the majority of the cellular SPCN pool is complexed with VASP in endothelial monolayers. SPCN–VASP interaction was further analyzed by confocal immunofluorescence microscopy in confluent ECV304 ECs (Takahashi et al., 1990). VASP was localized at cell–cell contacts, stress fibers, and focal adhesion sites. In horizontal and vertical cell sections, VASP colocalized with SPCN exclusively at cell–cell contacts, but not at focal adhesions or stress fibers (Fig. 2 C, a–c). Both proteins colocalized with the tight junctions marker zonula occludens protein-1 (ZO-1; Fig. 2 C, d–i). SPCN and VASP colocalized at junctions in other ECs such as EA.hy926 and HUVEC (unpublished data).

The SPCN SH3 domain specifically and directly interacts with VASP

SPCN contains an SH3 domain (Bennett and Baines, 2001). Because VASP binds to the SH3 domain of Abl (Ahern-Djamali et al., 1999), we analyzed SPCN SH3 domain (SPCN_SH3, residues E970–D1025) binding to VASP. SPCN_SH3 was cloned, expressed as a GST-fusion protein, and used in pull-down experiments. SPCN_SH3 (but not GST alone) precipitated VASP from cell lysates of confluent EA.hy926 and ECV304 (Fig. 3 A). We used immortalized ECs from microvessels of VASP-null (EC-VASP$^{-/-}$) and wild-type mice (EC-VASP$^{+/+}$). A VASP signal was only detected in SPCN_SH3 precipitates from EC-VASP$^{+/+}$ mice, confirming the specificity of anti-VASP antibodies (Fig. 3 B). To exclude that VASP binding to SPCN_SH3 is indirect, we analyzed purified recombinant proteins in a cell-free system. SPCN_SH3 specifically precipitated VASP (Fig. 3 D, left lanes).

SH3 domains are versatile protein interaction modules, which bind to proline-rich ligands with moderate affinity and selectivity (Mayer, 2001). To analyze the specificity of VASP binding to SPCN_SH3, we compared VASP binding to SPCN-related SH3 domains that were selected with the SH3-SPOT algorithm. This algorithm predicts complex formation of VASP with SH3 domains ranging from 0 (no affinity) to 1 (maximum affinity; Brannetti et al., 2000). The N- and C-terminal SH3 domains of VAV1 (0.9075 and 0.8375), and the SH3 domains of Abl (0.8992) and SPCN (0.8916) had the highest score for VASP binding.

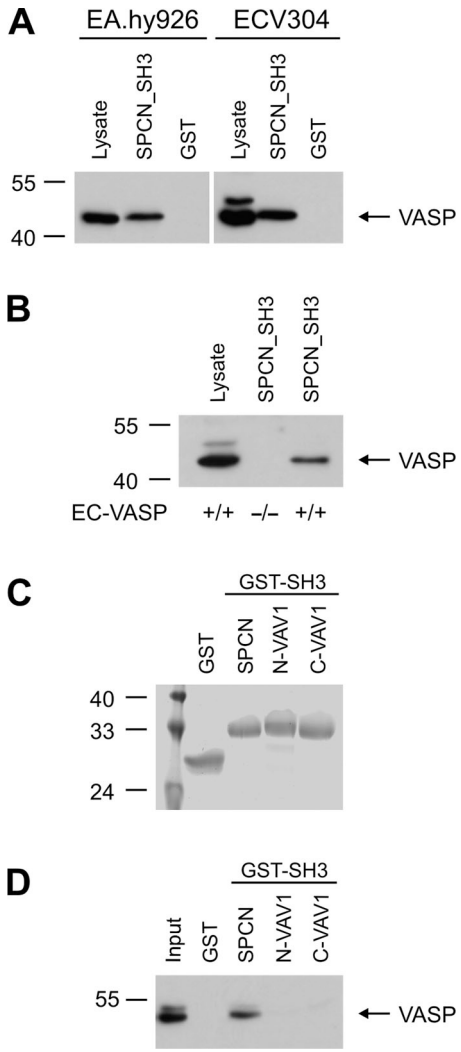

Figure 3. **The SPCN SH3 domain specifically and directly interacts with VASP.** (A) Immobilized GST-SPCN_SH3 protein or GST alone was incubated with confluent EA.hy926 (left) or ECV304 (right) cell lysates. Pulled down proteins were probed by Western blotting with anti-VASP antibodies. For control, cell lysates (Lysate) were applied. (B) Lysates from EC-VASP$^{+/+}$ and EC-VASP$^{-/-}$, were precipitated with SPCN_SH3 and probed as in A. (C) Coomassie-stained gel of purified SH3 domains of SPCN and VAV1 fused to GST or GST alone. (D) Immobilized GST-SH3 domains of SPCN and VAV1 or GST alone were incubated with purified recombinant His_6-VASP. Precipitated protein was probed with His_6 antibodies in Western blots. His_6-VASP was applied as positive control (Input).

The interaction of VASP with Abl SH3 domain has been previously confirmed (Howe et al., 2002). We cloned the SH3 domains of VAV1 (Fig. 3 C), and in pull-down experiments, VASP exclusively bound to SPCN_SH3, but not to VAV1 SH3 domains or GST alone (Fig. 3 D). Together, our data demonstrate a specific and direct interaction of VASP with the SH3 domain of SPCN.

The SPCN SH3 domain binds to the triple GP_5 motif of VASP

To map the SPCN_SH3 binding site in VASP, two C-terminally truncated VSV-tagged VASP mutants were generated. VSV-EVH1-PRR lacks the EVH2 domain. VSV-EVH1 lacks the central PRR and the EVH2 domain (Fig. 4 A). SPCN_SH3 precipitates from mutant-transfected 293 EBNA cells were analyzed with anti-VSV antibodies. VSV-VASP and VSV-EVH1-PRR, but not VSV-EVH1, bound to SPCN_SH3 (Fig. 4 B), suggesting that the PRR mediates the VASP–SH3 domain interaction. To identify the SPCN_SH3 binding motif in the PRR, we used peptide scans (Fig. 4 C). Overlapping, 15-aa-long peptides, spanning VASP PRR (residues 114–224) were synthesized on a cellulose membrane and incubated with SPCN_SH3 fused to GST or with GST alone (60 nM each). Bound proteins were detected by Western blotting with an anti-GST antibody. GST did not bind specifically (not depicted). SPCN_SH3 interacted with peptides F2 (P^{165}PAGGPPPPPGPPPP^{179}) and, more prominently, with F8 (P^{171}PPPGPPPPPGPPPP^{185}; Fig. 4 C). Both peptides overlap with the VASP triple GP_5 motif (positions 169–186). Peptides E10, F3, F4, and F10, which are as proline-rich as F8, were negative for SPCN_SH3 binding, confirming the specificity of the interaction. Peptides A1–A4, which cover the single GP_5 motif in the N-terminal portion of the PRR (G^{117}PPPPP^{122}), did not bind to SPCN_SH3 (Fig. 4 C).

VASP prolines 177, 178, and 179 are crucial for the SPCN–VASP interaction

To pinpoint residues within the VASP triple GP_5 motif that are crucial for SPCN binding, residues in F8 were systematically changed to alanine (Fig. 4 D). Substitution of the prolines P171, P174, P182, P185, and glycines G175 and G181 did not affect SPCN_SH3–VASP binding. Exchange of P172, P173, P183, and P184 moderately decreased SH3 binding to VASP. In contrast, proline residues from the central GP_5 motif (P176-P180) were critical for SH3 binding and exchange of any of the residues 177, 178, or 179 abrogated SPCN_SH3 binding (Fig. 4 D). To evaluate the importance of the three prolines for SH3 binding to full-length VASP, we generated VASP point mutants (P177A, P178A, and P179A). P179A interaction with SH3 was weak compared with nonmutated VASP. Substitution of P177 or P178 completely abrogated VASP binding to SPCN_SH3 (Fig. 4 E). To test the importance of the GP_5 motif for SPCN binding in cells, we reconstituted EC-VASP$^{-/-}$ cells with His_6-tagged wild-type VASP or P177A, P178A, and P179A. SPCN bound to wild-type VASP in coprecipitation experiments (positive control), but substitutions within the central GP_5 motif impaired SPCN binding (Fig. 4 F).

PKA-mediated phosphorylation of VASP at S157 inhibits its interaction with SPCN

SPCN bound to VASP-AAA, but not to -DDE (Fig. 1), suggesting that VASP phosphorylation controls the SPCN–VASP interaction. Because VASP residues P177-P179 are located in proximity to the PKA phosphorylation site S157 (Fig. 4 C), we analyzed S157 phosphorylation for SPCN–VASP binding. Phosphorylation at S157 induces an electrophoretic mobility shift of the protein from 46 to 50 kD (Krause et al., 2003). We incubated purified His_6-tagged VASP with active PKA in vitro. Anti-VASP antibodies detected the completely S157-phosphorylated protein at 50 kD (pS157-VASP; Fig. 5 A). In our pull-down assay, SPCN_SH3 precipitated nonphosphorylated, but not PKA-phosphorylated VASP (Fig. 5 A). Consistently, PKA activity abolished

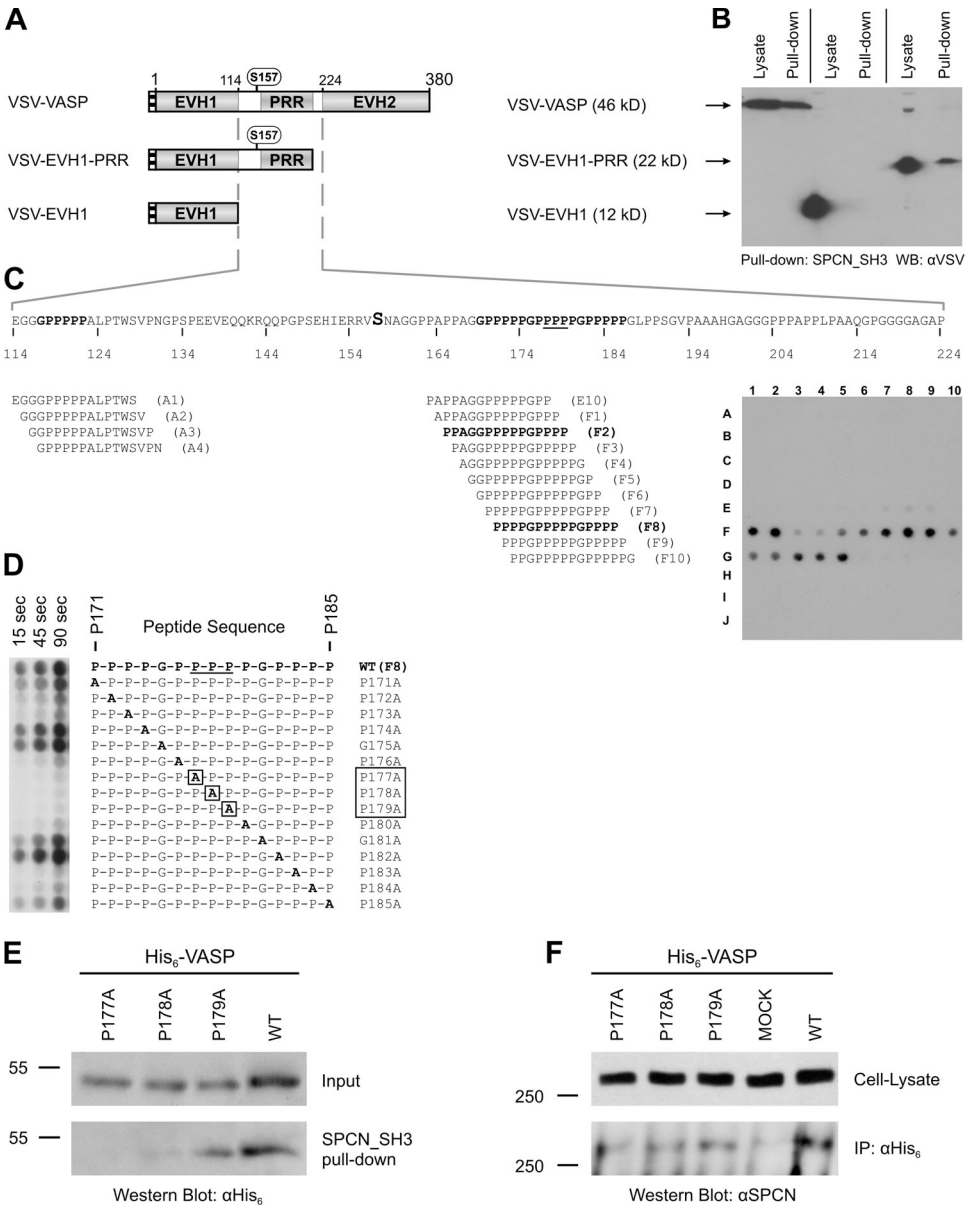

Figure 4. **The SPCN SH3 domain binds to the triple GP_5 motif of VASP.** (A) Schematic representation of VSV-tagged VASP and VASP mutants VSV-EVH1-PRR and VSV-EVH1. The PKA phosphorylation site S157 is printed in bold and highlighted in C. (B) Lysed VSV-VASP–, VSV-EVH1-PRR–, or VSV-EVH1–overexpressing cells were pulled down with SPCN_SH3. Precipitated material and lysates were probed with anti-VSV antibodies in Western blotting. (C) 15-mer peptides, which span the VASP PRR, were synthesized in a 10 × 10 peptide spot array (lines A–J and rows 1–10). VASP peptides were probed with GST-SPCN_SH3, followed by GST-specific antibodies, and bound antibody was detected with a secondary peroxidase-conjugated antibody. Peptides that bound to SPCN_SH3 (dark spots) are shown in bold. (D) Peptide F8 (P171-P185) or alanine mutants of this peptide were probed with SPCN_SH3. Alanine-substitution of P177-P179 eliminates SPCN_SH3 binding. Film exposure times are given above each lane. (E) Immobilized SPCN_SH3 was incubated with His_6-VASP (WT) or His_6-VASP mutants P177A, P178A, and P179A. Pulled down material was analyzed with His_6-specific antibodies. (F) EC-VASP$^{-/-}$ were transfected with His_6-VASP (WT), empty expression vector (MOCK), or His_6-VASP mutants P177A, P178A, and P179A. Cell lysates were immunoprecipitated (IP) with αHis_6 antibodies and precipitated material was blotted for SPCN (bottom). Cell lysates were run on the same gel and blotted for SPCN (top). Equal expression of VASP constructs is shown in Fig. 10 D.

SPCN_SH3 binding to mutant VASP-SAA (S239 and T278 sites are not phosphorylatable) in our pull-down assay (unpublished data). To investigate whether PKA-mediated VASP phosphorylation regulates SPCN–VASP interaction in cells, we treated His_6-VASP–overexpressing 293 EBNA cells with Rp-8-Br-cAMPs (PKA antagonist) or with forskolin (PKA activator). Cell lysates were precipitated with SPCN_SH3 and probed with anti-His_6 antibodies. SPCN_SH3 specifically pulled down nonphosphorylated VASP, but not the S157-phosphorylated protein (Fig. 5 B).

Phosphomimetic substitution of S157 blocks SPCN-VASP interaction

To address the contribution of the two VASP phosphorylation sites, S239 and T278, for SPCN–VASP complex formation, we generated VASP pseudophosphorylation mutants. Phosphorylation sites were either exchanged to acidic amino acids or to alanines (mimicking a constitutively phosphorylated or unphosphorylated residue, respectively). Fig. 5 C gives a schematic representation of the five mutants (VASP-DDE, -AAA, -DAA, -ADA,

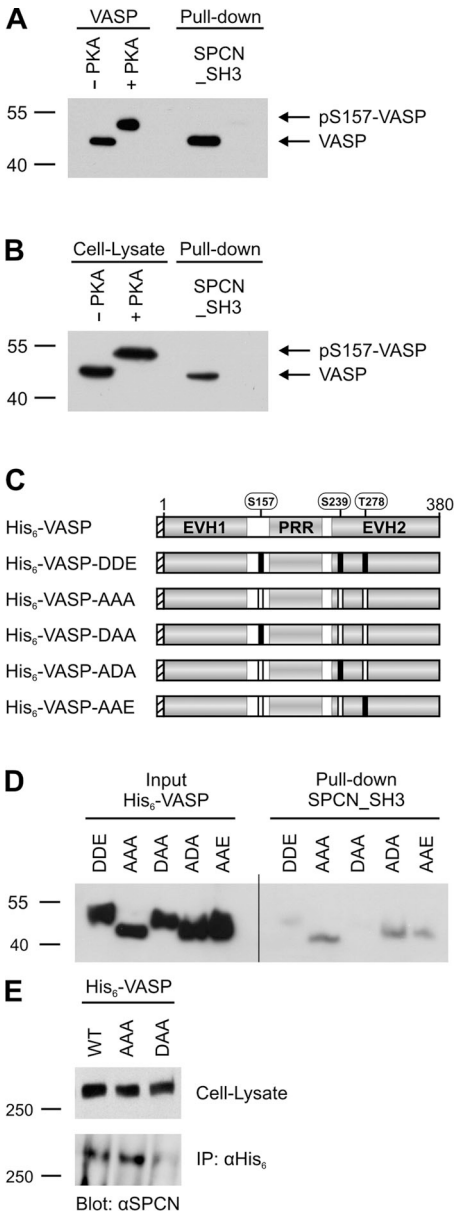

Figure 5. **PKA-mediated phosphorylation of VASP at S157 inhibits its interaction with SPCN.** (A) Purified His_6-tagged VASP was S157-phosphorylated (pS157-VASP) in vitro by PKA (+PKA) or left untreated (–PKA) and pulled down with immobilized SPCN_SH3. Precipitates were analyzed by Western blotting with His_6-specific antibodies. (B) His_6-tagged VASP was overexpressed in 293 EBNA cells and cells were either treated with a PKA inhibitor (Rp-8-Br-cAMPs, –PKA) or a PKA stimulator (forskolin, +PKA). Cells were lysed, incubated with immobilized SPCN_SH3, and complexes were analyzed with anti-His_6 antibodies (Pull-down). (C) Schematic representation of His_6-tagged VASP and mutants VASP-DDE, -AAA, -DAA, -ADA, and -AAE. In the mutants, phosphorylation sites S157, S239, and T278 were substituted by alanines (A, open boxes) or negatively charged acidic amino acids (D or E, filled boxes). (D) Purified His_6-tagged VASP-DDE, -AAA, -DAA, -ADA, and -AAE (left) was pulled down with immobilized SPCN_SH3 and precipitated proteins were analyzed with His_6-specific antibodies (right). Phosphorylation and phosphomimetic substitution of S157 induces a shift of VASP motility in SDS-PAGE. (E) EC-VASP$^{-/-}$ were transfected with His_6-VASP (WT) or His_6-tagged VASP-AAA or -DAA. Cell lysates were immunoprecipitated with αHis_6 antibodies and precipitated material was blotted for SPCN. Equal expression of VASP constructs is shown in Fig. 10 E.

and -AAE). In pull-down experiments, SPCN_SH3 interacted with recombinant VASP-AAA, -ADA, and -AAE, but not with VASP-DDE or -DAA, demonstrating that a negative charge at position 157 abolishes SPCN–VASP binding, whereas pseudo-phosphorylations at positions 239 and 278 did not affect SPCN–VASP complex formation (Fig. 5 D). To confirm the role of negative charges at position 157 for SPCN–VASP binding in cells, we reconstituted EC-VASP$^{-/-}$ with wild-type VASP, VASP-DAA, or -AAA. SPCN bound to VASP-AAA, but not to -DAA, in coimmunoprecipitation experiments, supporting a negative-regulation of SPCN–VASP binding by S157 phosphorylation (Fig. 5 E).

SPCN colocalizes with S157 VASP, but not with phospho-S157 VASP, in contacting ECs

To investigate cellular functions of PKA-mediated S157 phosphorylation for SPCN–VASP complex formation, we analyzed the subcellular distribution of total-VASP, pS157-VASP, and SPCN in ECs. Because pS157-VASP levels are dynamically regulated during actin-based processes (Howe et al., 2002), we investigated subcellular localizations of the proteins dependent on cell density. We investigated sparse cells (which have few contact sites; Fig. 6 A), contacting cells (where about half of the cells have cell–cell junctions; Fig. 6 B), and confluent cells (which have maximal contact sites; Fig. 6 C). In sparse cells, total-VASP and pS157-VASP were predominantly found at focal adhesions and in more punctuate patterns at developing contacts. Both antigens colocalized almost completely at these sites (Fig. 6 A, a, b, and d). In contrast, SPCN was enriched at the cell periphery and did not colocalize with total-VASP or with pS157-VASP (Fig. 6 A, c, e, and f). In contacting cells, subcellular VASP distribution was strikingly different. A portion of total-VASP was still localized at focal adhesions, but a second VASP pool at cell–cell contacts appeared (Fig. 6 B, a). The membrane-associated VASP fraction colocalized with SPCN and was not S157 phosphorylated (Fig. 6 B, a–e). In contacting cells, S157 phosphorylation was lower compared with sparse cells. pS157-VASP was mainly found at focal adhesions, and colocalization with SPCN was minor (Fig. 6 B, b, c, and f). In confluent cells, total-VASP colocalized with SPCN at cell–cell junctions (Fig. 6 C, a, c, and e), and pS157-VASP was almost undetectable (Fig. 6 C, b, d, and f; note that anti–pS157-VASP antibodies unspecifically stain cell nuclei). To confirm that VASP phosphorylation disappears with formation of cell–cell contacts, we quantified VASP phosphorylation by Western blotting using phosphorylation status-specific antibodies directed to the sites S157, S239, and T278, respectively (Fig. 7, A and B). ECV304 cells were detached, and equal cell numbers were seeded and allowed to grow for various times before lysis. 3 h after seeding, cells were sparse, lamellipodia were visible, and cell–cell contacts were virtually absent. Within 24 h, about half of the cells developed cell–cell contacts, and after 48 h cells were confluent (Fig. 7 C). Consistent with high pS157 levels in detached cells (Howe et al., 2002), VASP S157 phosphorylation was high in freshly seeded cells. S157 phosphorylation level decreased time-dependently when cells established cell–cell contacts.

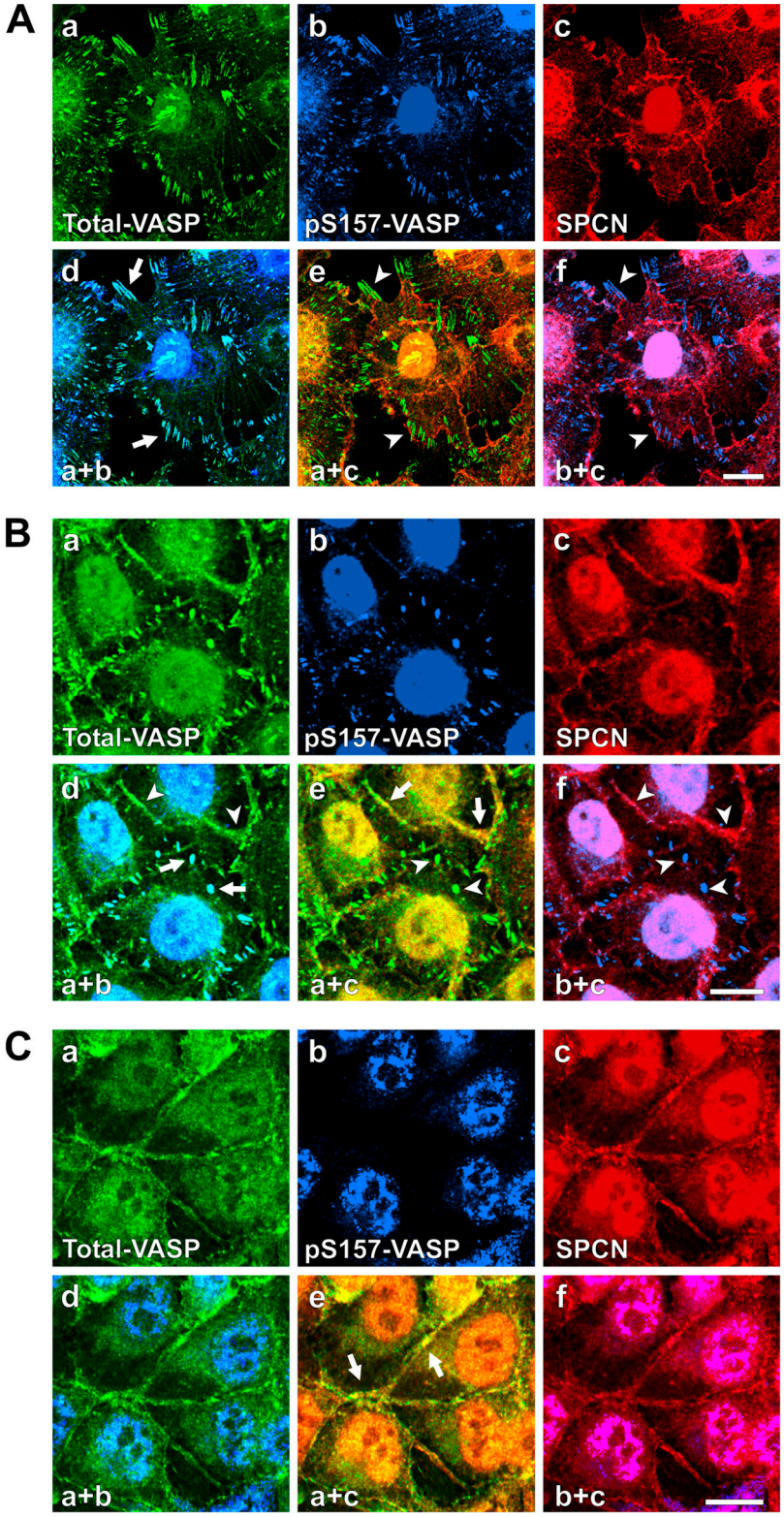

Figure 6. **SPCN colocalizes with S157-VASP, but not with phospho-S157-VASP in contacting ECs.** Confocal immunofluorescence images of sparse (A), contacting (B), or confluent (C) ECV304 cell stained for total-VASP (a, green), pS157-VASP (b, blue), and SPCN (c, red). (A) In sparse cells, total-VASP and pS157-VASP were found at focal adhesions (d, arrows). SPCN was enriched at the cell periphery and did not colocalize with total-VASP or pS157-VASP (e and f, arrowheads). (B) In contacting cells, total-VASP was found at focal adhesions, where it colocalized with pS157-VASP, and at cell–cell contacts, where it colocalized with SPCN (d and e, compare arrows and arrowheads). pS157-VASP was mainly seen at focal adhesions and did not colocalize with SPCN (f, arrowheads). (C) In confluent cells, pS157-VASP was almost not detectable (b; note: anti–pS157-VASP antibodies unspecifically stain cell nuclei). Total VASP was predominantly localized at cell–cell contacts, where it colocalized with SPCN (e, arrows). Arrows indicate sites with colocalization; arrowheads indicate sites without colocalization. Bars, 15 μm.

Only trace amounts of pS157-VASP were detected in confluent cells. In contrast, phosphorylation levels of S239 and T278 were not dependent on confluency state. As control for intact PKA signaling, we stimulated confluent cells with 10 μM forskolin, which largely increased S157 phosphorylation (Fig. 7, A and B). Forskolin treatment had no visible effect on the morphology of contacts in ECV304 cells as analyzed by phase-contrast microscopy. We tested whether SPCN–VASP complex formation depends on PKA activity and cell confluency using coimmunoprecipitation. VASP precipitated SPCN from confluent cells, but SPCN–VASP complexes were virtually absent in sparse and PKA-activated confluent cells (Fig. 7 D).

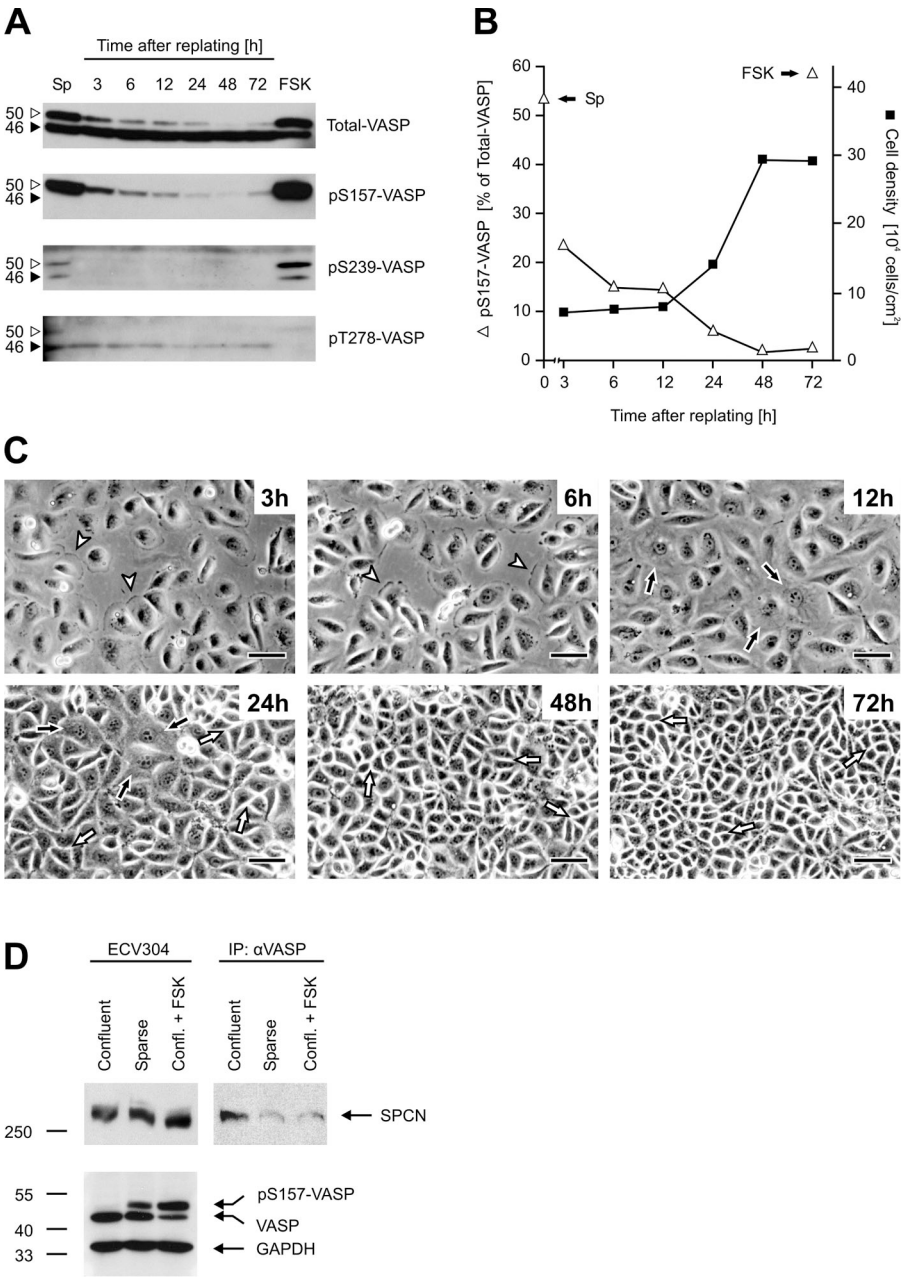

Figure 7. **VASP S157 phosphorylation decreases with the formation of cell–cell contacts.** Confluent ECV304 cells were detached, and a constant number of cells (7.5×10^4 cells/cm^2) was replated and grown for the indicated times before cells were analyzed for VASP phosphorylation (A and B), imaged by phase-contrast microscopy (C), or immunoprecipitated with αVASP antibodies (D). (A) Western blots with anti-VASP or phosphorylation-specific antibodies against pS157-, pS239-, and pT278-VASP, respectively. As control for maximal PKA stimulation, cells were either detached and incubated in suspension for 15 min (Sp) or treated with 10 μM forskolin (FSK) 72 h after replating. Open triangles represent S157-phosphorylated VASP (50 kD), and filled triangles indicate S157 nonphosphorylated VASP form (46 kD). (B) Kinetics of VASP S157 phosphorylation levels (open triangles) dependent on density of ECV304 cells (filled squares). Magnitude of pS157-VASP (relative to the amount of total-VASP) was quantified from Western blots (in A) by densitometric scans. pS157-VASP level of suspended (Sp) or FSK-treated cells are indicated. (C) Phase-contrast images of ECV304 cells. 3 and 6 h after seeding, cells were sparse and lamellipodia were visible (arrowheads). 12 h after replating, cells were maximally spread. Approximately half of the cells remained in this state 24 h after seeding (closed arrows), whereas the other half formed cell–cell contacts (open arrows). After 48 and 72 h, a confluent EC monolayer formed. Bars, 30 μm. (D) Lysates of confluent, sparse, or FSK-treated confluent ECV304 cells were immunoprecipitated with αVASP antibodies. Lysates were analyzed by Western blotting with αSPCN or αVASP antibodies (left), and precipitated material was probed with αSPCN antibodies (right). GAPDH served as loading control.

Ectopic expression of SPCN_SH3 recruits VASP and promotes cortical actin formation

To analyze the function of the SPCN–VASP interaction for cell–cell contact formation, we ectopically expressed SPCN SH3 domain at endothelial junctions and investigated VASP distribution and cortical cytoskeleton formation. SPCN_SH3 was cloned to the C terminus of claudin-5 (Cl), which is an integral membrane protein of tight junctions (Tsukita et al., 2001), and a VSV-tag was inserted in between (Cl-VSV-SH3). We used a VSV-tagged Cl construct lacking SH3 as control (Cl-VSV). Expression of the constructs in ECV304 cells was confirmed by Western blotting with VSV-specific antibodies (Fig. 10 A, inset). Anti-VSV antibodies detected Cl-VSV-SH3 and Cl-VSV almost exclusively at the plasma membrane (Fig. 8, A and D and G and J). In Cl-VSV-SH3–expressing cells, VASP was enriched at the plasma membrane (Fig. 8, B and E), and overlap of the proteins in this compartment was >80% (Fig. 8, C and F). In contrast, colocalization of Cl-VSV and VASP was minor (<35%; Fig. 8, I and L). Comparison of VASP localization in Cl-VSV-SH3– and Cl-VSV–overexpressing cells suggested that the SPCN SH3 domain is sufficient to initiate VASP translocation (Fig. 8, B and E vs. H and K). In Cl-VSV-SH3–transfected cells, VASP was gone from stress fibers, recruited to cell–cell junctions, and colocalized with SPCN_SH3. Pull-down and coprecipitation experiments have demonstrated direct and specific binding of VASP to the SPCN SH3 domain. If the claudin-fused SH3 domain exerts effects similar to those of full-size SPCN, we would predict that the individual domain competes with SPCN–VASP complex formation. To test this hypothesis, we

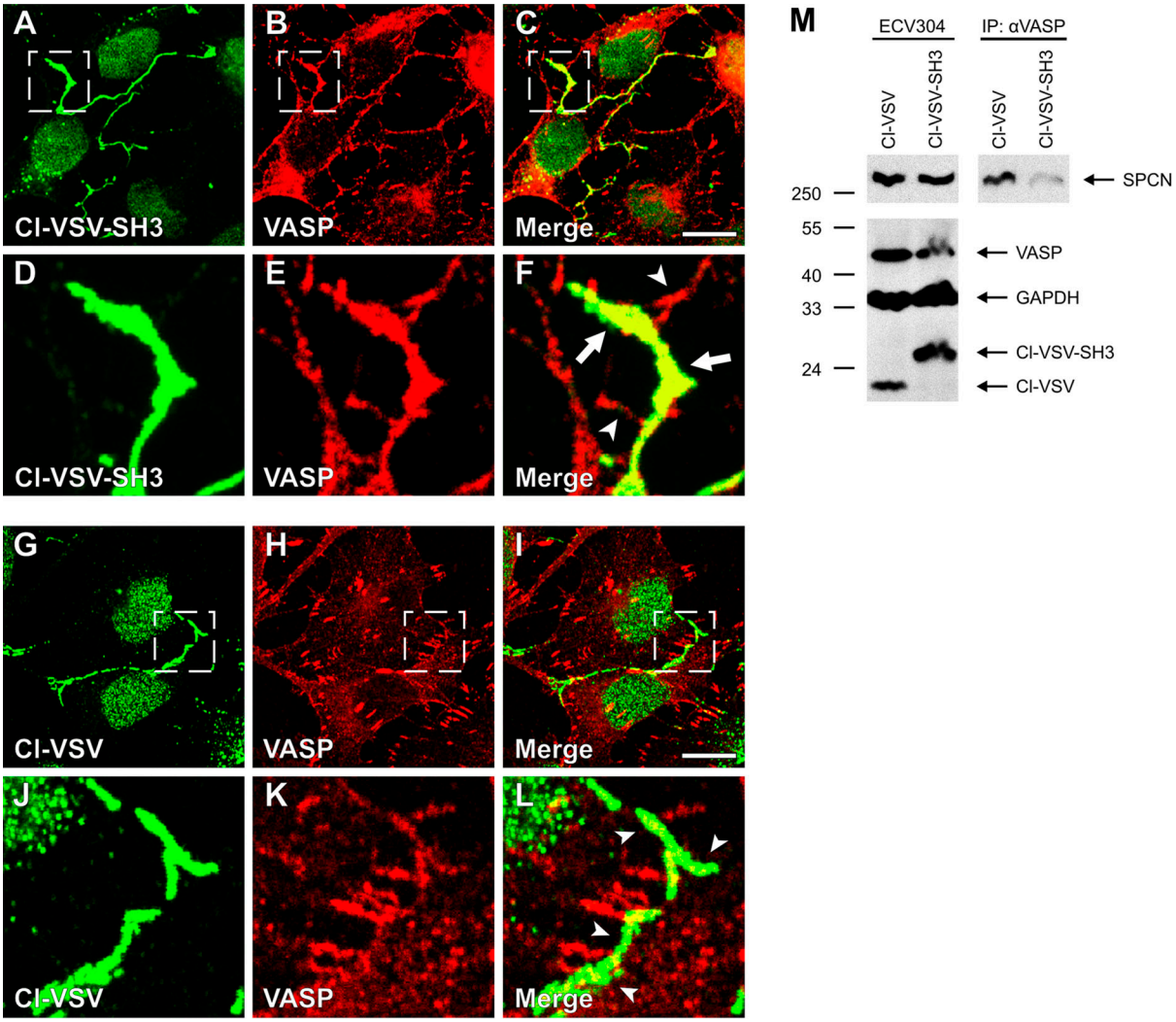

Figure 8. **Ectopic expression of SPCN_SH3 recruits VASP to the plasma membrane.** ECV304 cells were transfected with the SPCN SH3 domain fused to VSV-tagged claudin-5 (Cl-VSV-SH3) or with VSV-tagged claudin-5 alone (Cl-VSV, control), fixed, and processed for confocal immunofluorescence microscopy. Cells were stained for Cl-VSV-SH3 (A and D; green), Cl-VSV (G and J; green), and VASP (B, E, H, and K; red). Images D–F and J–L show magnified views of the indicated areas in the preceding images. Arrows in the overlays C, F, I, and L indicate sites with colocalization; arrowheads indicate sites without colocalization. Bars, 15 µm. (M) Lysates of Cl-VSV– and Cl-VSV-SH3–transfected ECV304 cells were immunoprecipitated (IP) with αVASP antibodies. Lysates were analyzed by Western blotting with anti-SPCN, -VASP, and -VSV antibodies (left), and precipitated material was analyzed with anti-SPCN antibodies (right). GAPDH served as loading control.

precipitated VASP from Cl-VSV– and Cl-VSV-SH3–transfected ECV304 cells and probed for SPCN. VASP precipitated less SPCN from Cl-VSV-SH3–expressing compared with Cl-VSV–expressing cells (Fig. 8 M).

What is the consequence of SPCN–VASP complex formation for perijunctional actin filament assembly? Cl-VSV-SH3 expression promoted cortical F-actin assembly, which was visualized with fluorescent phalloidine (Fig. 9, B and E). The formation of actin fibers was prominent at Cl-VSV-SH3–positive membrane sections (Fig. 9, A, C, D, and F; arrows and arrowheads indicate Cl-VSV-SH3–positive or –negative areas, respectively), and signals overlapped by >95% at these sites. In contrast, although Cl-VSV localized to the plasma membrane (Fig. 9, G and J), overexpression did not initiate cortical actin cytoskeleton formation (Fig. 9, H and K). Colocalization of Cl-VSV and actin was low (<40%; I and L). As judged from fluorescence signal intensity, cortical actin fiber deposition was increased by more than twofold in Cl-VSV-SH3– over Cl-VSV–expressing cells.

Importance of SPCN-VASP complexes for endothelial barrier function

We investigated the function of SPCN–VASP interaction for permeability control in the endothelium. Stability of IEJs was analyzed in confluent cells with the calcium-switch model. Under basal conditions, cell–cell contacts are closed (Mehta and Malik, 2006). Complexation of extracellular calcium ions abrogates cell–cell adhesion forces and initiates transition of cortical actin rings to stress fibers that culminates in disruption of cell–cell contacts and gap formation in the monolayer (Fig. S1, available at http://www.jcb.org/cgi/content/full/jcb.200709181/DC1). Opening of IEJs is followed by transition of macromolecular

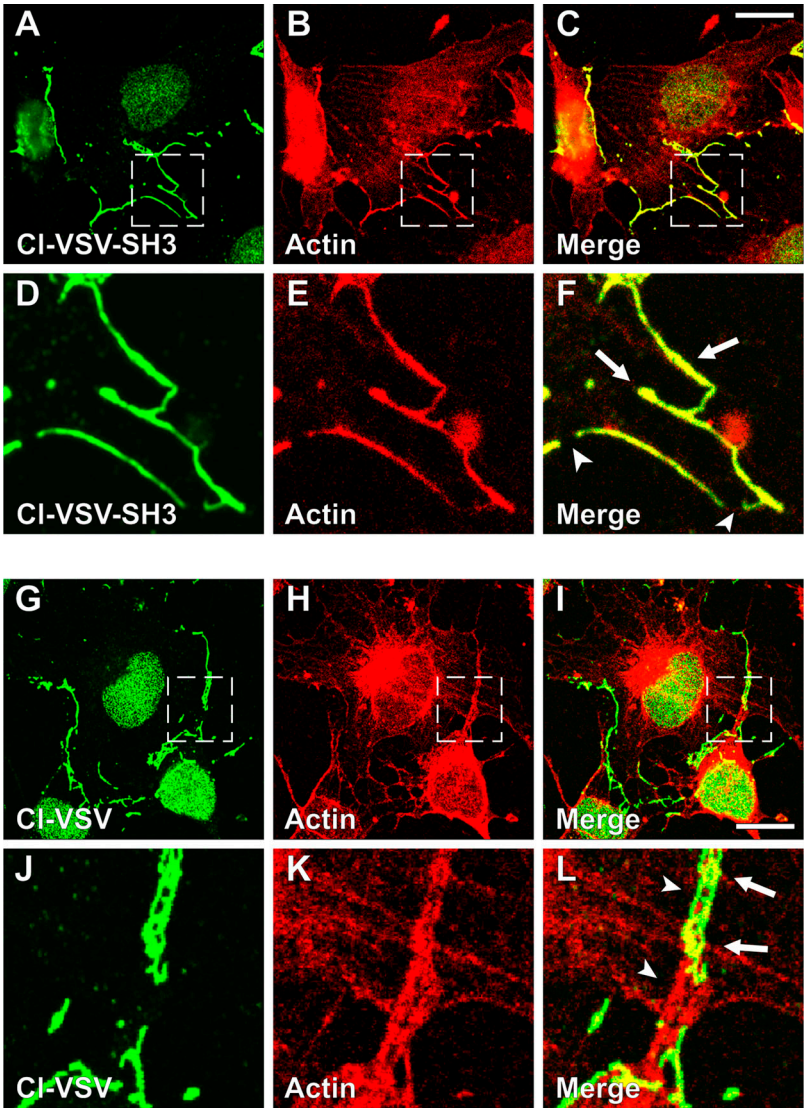

Figure 9. **Ectopic expression of SPCN_SH3 promotes cortical actin formation.** ECV304 cells were transfected with Cl-VSV-SH3 or Cl-VSV (control), and analyzed by confocal immunofluorescence microscopy. Cells were stained for Cl-VSV-SH3 (A and D), Cl-VSV (G and J), and actin (B, E, H, and K). Images D–F and J–L are magnified views of the indicated areas in the preceding images. Arrows in the overlays (C, F, I, and L) indicate sites with colocalization; arrowheads indicate sites without colocalization. Bars, 15 μm.

tracers (Citi, 1992). ECV304 cells were seeded on porous filters and transfected with Cl-VSV-SH3 or Cl-VSV (transfection rates 30–37%) before FITC-albumin addition to apical chambers. Western blot analyses revealed equal expression levels of the constructs (Fig. 10 A, inset). Basal permeability of monolayers was recorded for 2 h. After removal of extracellular calcium (4 mM EGTA; Citi, 1992), transition of fluorescent tracer into the lower chambers was determined for an additional 3.5 h. FITC-albumin leakage through Cl-VSV-SH3–overexpressing cell monolayers was significantly lower as compared with Cl-VSV–transfected cells (0.15 vs. 0.11 for 3.5 h; $n = 7$; $P < 0.05$; Fig. 10 A). We analyzed the function of SPCN–VASP complexes for paracellular permeability in EC-VASP$^{+/+}$ and EC-VASP$^{-/-}$ cells (Fig. 10 B, inset). In the calcium-switch assay, permeability of EC-VASP$^{-/-}$ exceeded EC-VASP$^{+/+}$ monolayers (0.39 vs. 0.18 for 2 h; $n = 7$; $P < 0.05$; Fig. 10 B), suggesting that VASP deficiency interferes with the stability of IEJs. To test this hypothesis in whole animals, we analyzed VASP-null mice in a skin vascular leakage model. Edema formation was induced by subdermal application of the inflammatory mediator bradykinin (Renne et al., 2005). Tracer measurements revealed that bradykinin-induced vascular leakage was significantly increased in VASP$^{-/-}$ over wild-type mice (4.9- vs. 3.2-fold of saline; $n = 7$; $P < 0.05$; Fig. 10 C). To specifically address the impact of PKA-regulated SPCN–VASP interaction for inter-endothelial adhesion and permeability, we used a rescue strategy. EC-VASP$^{-/-}$ cells were reconstituted with SPCN binding-defective VASP mutants P178A, P177A, P179A, (Fig. 4, E and F) or wild-type protein and subjected to a calcium switch. Consistent with nontransfected cells, FITC-albumin leakage was significantly higher in mock-transfected EC-VASP$^{-/-}$ over EC-VASP$^{+/+}$ cells (0.67 vs. 0.31 for 3 h; $n = 6$; $P < 0.05$; Fig. 10, D and E). Expression of wild-type VASP in EC-VASP$^{-/-}$ cells reduced leakage (0.51 vs. 0.67 of mock for 3 h; $n = 6$; $P < 0.05$; transfection rates were 23–28% as determined by FACS analyses). Reconstitution of EC-VASP$^{-/-}$ cells with SPCN binding-defective mutants P177A, P178A, and P179A had minor effects on permeability (0.59, 0.63, 0.58 vs. 0.51 of wild-type VASP, 3 h, $n = 6$, $P < 0.05$; Fig. 10 D). Finally, we tested the relevance of VASP S157 phosphorylation for SPCN–VASP-mediated

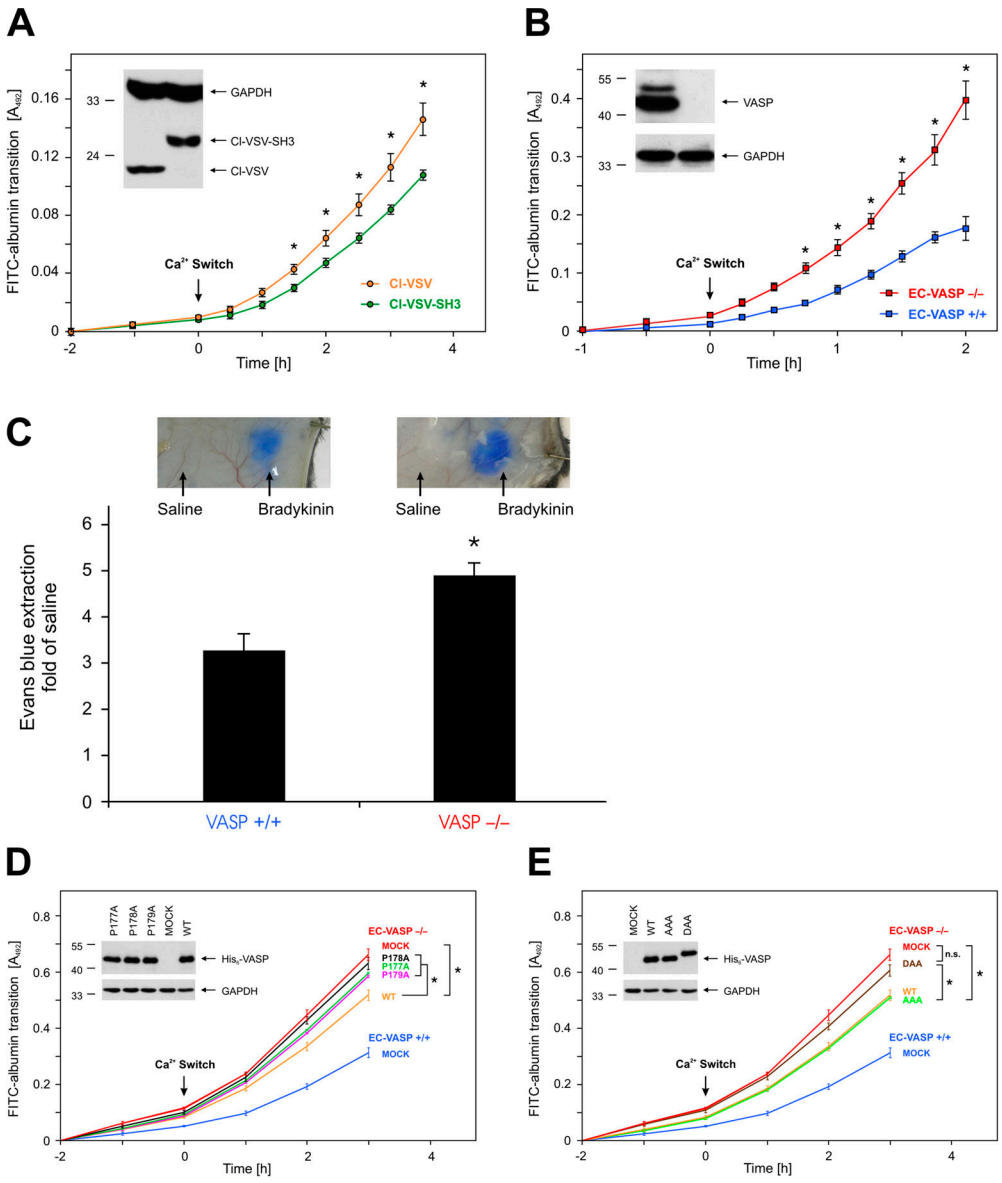

Figure 10. **Importance of SPCN–VASP complexes for endothelial barrier function.** Permeability of Cl-VSV– (orange) or Cl-VSV-SH3–overexpressing (green) confluent ECV304 cells (A), or EC-VASP$^{-/-}$ (magenta) or EC-VASP$^{+/+}$ (blue; B) were analyzed in the calcium-switch model. Absorbance at 492 nm in the lower compartments determined transition of FITC-albumin tracer through the monolayers. Arrows indicate EGTA application. Means and SE are given. $n = 7$. *, $P < 0.05$. (insets) Western blots of lysed Cl-VSV– or Cl-VSV-SH3–transfected ECV304 cells, probed with anti-VSV tag antibodies (A) or EC-VASP$^{+/+}$ or EC-VASP$^{-/-}$ cells analyzed with anti-VASP antibodies. GAPDH served as loading control (B). (C) Comparison of bradykinin-induced vascular leakage in VASP$^{-/-}$ and wild-type mice skin. In Evans blue–injected mice, edema formation was induced by subdermal application of 100 μM bradykinin or saline. Evans blue extravasation was quantified photometrically. Values are blotted relative to saline injection. $n = 7$. *, $P < 0.05$. (D and E) Permeability of EC-VASP$^{-/-}$, transfected with His$_6$-VASP (WT, orange) and (D) His$_6$-VASP mutants P177A (light green), P178A (black), and P179A (magenta) or (E) His$_6$-tagged VASP-AAA (green) or -DAA (brown) was analyzed in the calcium-switch model. Permeability of mock-transfected EC-VASP$^{-/-}$ and EC-VASP$^{+/+}$ are given in red and blue, respectively. Mean ± the SEM. $n = 6$. *, $P < 0.05$. (insets) Western blot of lysed EC-VASP$^{-/-}$ transfected with indicated VASP constructs and probed with anti-His$_6$ antibodies. GAPDH is loading control.

barrier function. Reconstitution of EC-VASP$^{-/-}$ cells with VASP-AAA rescued leakage similarly to wild-type protein (0.50 and 0.51 at 3 h, $n = 6$, $P < 0.05$; Fig. 10 E). In contrast, expression of the SPCN binding-defective mutant VASP-DAA that mimics S157 phosphorylated VASP, failed to rescue barrier function (0.60 vs. 0.67 of mock-transfected cells for 3 h; $n = 6$; P = n.s.; Fig. 10 E). Together, the data indicate that SPCN–VASP complexes stabilize EC–cell contacts with implication for vascular barrier integrity, and that VASP S157 phosphorylation regulates this process.

Discussion

The endothelial lining of the vessel wall acts as a permeable filter, which allows selective transition of water, solutes, macromolecules, and cells from the luminal to the abluminal side of the barrier. Paracellular permeability is regulated by a complex interplay of cellular adhesive and counteradhesive forces, which are generated by transmembrane adhesion molecules, actin filament assembly, and actinomyosin molecular motors. This study links the spectrin-based skeleton to remodeling of the actin filament network.

SPCN–VASP assemble perijunctional multiprotein complexes

VASP was originally identified in platelets, and VASP activity participates in a variety of actin-based processes, such as adhesion or spreading in these cells. Subsequently, the importance of VASP-driven actin assembly was established in other cell lines, including keratinocytes (Vasioukhin et al., 2000), leukocytes (Lawrence and Pryzwansky, 2001), fibroblasts (Bear et al., 2002), smooth muscle (Chen et al., 2004), epithelial cells (Lawrence et al., 2002), and ECs (Price and Brindle, 2000), in vessels of animal models and in humans (Munzel et al., 2003). In epithelial and keratinocyte monolayers, proteins of the Ena/VASP family participate in cell–cell adhesion and formation of adhesion zippers by a mechanism that requires α-catenin (Vasioukhin et al., 2000) and cadherin (Scott et al., 2006). Ena/VASP proteins promote actin polymerization and assembly and several models of VASP-mediated F-actin control have been proposed, including regulation of nucleation, bundling, branching, and capping (Barzik et al., 2005; Schirenbeck et al., 2006). It is the interaction with SPCN that may give the spacing for VASP-driven plasma membrane–associated actin filament assembly. Bound to SPCN, VASP assembles multiprotein complexes with IEJ components. VASP and the tight junction protein ZO-1 co-immunoprecipitate from lysates of ECs (Comerford et al., 2002). However, the interaction appears to be indirect (Lawrence et al., 2002). SPCN interactions with VASP (Figs. 1–3) and with ZO-1 (Tsukamoto and Nigam, 1997) could bridge the molecules. α-Catenin appears to be another component of SPCN–VASP multiprotein complexes. In α-catenin–deficient keratinocytes, VASP localization to cell–cell borders is impaired, suggesting that α-catenin interacts with VASP at sites of intercellular adhesion (Vasioukhin et al., 2000). Evidence for a direct interaction of α-catenin and VASP is missing, and adaptors might link the proteins. Because α-catenin directly binds to spectrins (Pradhan et al., 2001), which in turn interact with VASP (Fig. 2), lack of α-catenin–SPCN interaction in α-catenin–null cells might account for defective recruitment of VASP to cell–cell contacts. Consistently, spectrin tetramer assembly at the plasma membrane has been shown to be diminished in cells expressing an α-catenin mutant that fails to associate with the plasma membrane (Pradhan et al., 2001). In summary, the data argue for large complexes of junctional proteins, spectrin, and VASP, and possibly other unidentified proteins, at cell–cell contacts.

SPCN SH3 domain mediates interaction with VASP

One of the key findings of this study is that the spectrin SH3 domain, which is unique to α-spectrins and not found in other isoforms, specifically interacts with VASP. PKA-mediated phosphorylation controls SPCN_SH3–VASP interaction (Fig. 5). Consistently, binding of VASP and the Ena/VASP protein family member EVL to SH3 domains of Abl and Src is dependent on PKA activity (Ahern-Djamali et al., 1999; Lambrechts et al., 2000; Howe et al., 2002). Yeast two-hybrid screens indicated EVL interaction with SPCN (Rotter et al., 2005), supporting the coupling of spectrin-based membrane skeletons with proteins involved in actin dynamics. ECV304 ECs do not express EVL, as revealed by Western blotting and immunofluorescence microscopy (Fig. S2, available at http://www.jcb.org/cgi/content/full/jcb.200709181/DC1), excluding a modulatory role of EVL on SPCN–VASP complex formation in our system. In yeast nucleus, VASP did not to bind to the bait SPCN_SH3 (Bournier et al., 2006). Because active PKA accounts for high kinase activity in yeast nuclei (Griffioen and Thevelein, 2002), PKA could phosphorylate VASP at S157 and inhibit SPCN_SH3–VASP interaction. Within the VASP PRR, peptide scans identified sequences comprising the triple GP_5 (F2, F8; Fig. 4 C) as important for SPCN_SH3 binding. It is not clear whether both peptides contribute equally to SPCN–VASP complex formation or whether one harbors the preferred SH3 binding site of full-length VASP. Possibly, the two peptides together form a surface for SPCN_SH3 docking. Cooperative binding is known for other proline recognition domains (Li, 2005). SH3 domains interact with proline-rich ligands with consensus sequences + xΦPxΦP or ΦPxΦPx + (class I or class II ligands, where x is any, Φ is a hydrophobic, and + is a positively charged amino acid, respectively; Kay et al., 2000). Because peptides F2 and F8 do not contain positively charged amino acid residues, SPCN_SH3 appears to belong to the atypical SH3 domains. These domains prefer ligands in which hydrophobic residues contact the specificity pocket (Mayer, 2001). Consistently, SPCN SH3 domain was shown to interact with the peptide PPLAL-TAPPPA at the C terminus of rat amiloride-sensitive epithelial Na^+ channel α subunit (αrENaC), which lacks a positively charged amino acid (Rotin et al., 1994). Furthermore, the Abl SH3 domain, which binds to VASP (Howe et al., 2002), is also an atypical SH3 domain (Mayer, 2001). SPCN_SH3 binds to the Ena/VASP protein family member EVL, but the binding site was not mapped (Rotter et al., 2005). EVL lacks a triple GP_5 motif that mediates VASP binding to SPCN (Fig. 4). The other family member Mena does not bind to SPCN_SH3 (Bournier et al., 2006). Pull-downs, coprecipitations, and peptide scan data roughly suggest a 1:1 stoichiometry of VASP and spectrin in the complex. Because VASP and spectrin are tetrameric in cells, the exact binding mechanism remains speculative. EVL binding to Abl and nSrc SH3 domains, but not to profilin is abolished by PKA-mediated phosphorylation of the S157 equivalent site (Lambrechts et al., 2000). Consistently, when regulated by PKA activity, SPCN_SH3 binds to the VASP triple GP_5 motif (Figs. 4 and 5). Profilin binding to VASP was thought to be mediated by the triple GP_5 motif (Kang et al., 1997); however, recent structural analyses challenged this hypothesis (Ferron et al., 2007). We tested whether profilin competes with SPCN SH3 domain for VASP binding. In competition experiments, profilin did not interfere with SPCN–VASP complex formation (Fig. S3, available at http://www.jcb.org/cgi/content/full/jcb.200709181/DC1), supporting the notion of Ferron et al. (2007) that high-affinity profilin/VASP binding is mediated by a more C-terminal site, which is different from the triple GP_5 motif.

Regulation and functional importance of SPCN–VASP complexes

Our study provides evidence that VASP regulates actin formation in defined subcellular compartments. Targeting of VASP to these sites is regulated by PKA activity. In sparse ECs, VASP is

PKA-phosphorylated at S157 and not bound to SPCN at the plasma membrane (Figs. 6 and 7). S157-phosphorylated protein is enriched at focal adhesions and could interact with vinculin, zyxin, and migfilin at these sites (Drees et al. 2000; Hoffman et al., 2006). When ECs establish cell–cell junctions, pS157 levels decrease and SPCN–VASP complexes form (Figs. 6 and 7). At the plasma membrane, VASP participates in the formation of a cortical actin ring (Mehta and Malik, 2006). The cortical actin cytoskeleton is pivotal for the integrity and stability of IEJs, which in turn is essential for EC barrier function (Ermert et al., 1995). Consistently, vascular leakage is increased in VASP-deficient mice (Fig. 10 C). The data support previous observations that indicated a role of VASP for actin assembly at cell–cell contact sites in PKA-treated and hypoxia-activated ECs (Comerford et al., 2002; Rosenberger et al., 2007). Consistent with the relevance of VASP for barrier function in stressed endothelium, VASP-null mice do not suffer from constitutive (basal) swellings. Only in activated vessels is permeability increased (Fig. 10 C).

In summary, we have identified a new mechanism for formation of cortical actin cytoskeletons. SPCN–VASP complexes trigger perijunctional actin filament assembly, and PKA-driven VASP phosphorylation at S157 inhibits this process. SPCN–VASP interactions improve cell–cell adhesion, with implications for endothelial barrier permeability.

Materials and methods

Animals

Generation of VASP-deficient mice has been previously reported (Hauser et al., 1999). Animals were backcrossed for more than eight generations to C57BL/6J background. All experiments and animal care were approved by the Regierung von Unterfranken.

Cell culture

EA.hy926 cells were cultivated as previously described (Renne et al., 2005). ECV304 and 293 EBNA cells were grown in DME containing 4.5 g/liter glucose supplemented with 10% FBS. Wild-type and VASP-deficient murine microvascular myocardial ECs (EC-VASP$^{+/+}$ or EC-VASP$^{-/-}$, respectively) were generated, characterized, and cultured as previously described (Golenhofen et al., 2002; Schlegel et al., 2007). 293 EBNA, ECV304, EC-VASP$^{+/+}$, and EC-VASP$^{-/-}$ cells were transiently transfected with Lipofectamine 2000 (Invitrogen) and analyzed 12–36 h later. To correlate VASP phosphorylation with cell density, ECV304 cells were detached with trypsin-EDTA and collected into medium containing 10% FBS. Cells were maintained in suspension (Sp) for 15 min before lysis or replated on tissue culture plates (7.5×10^4 cells/cm^2). 3, 6, 12, 24, 48, or 72 h after seeding, adherent cells were photographed, lysed in SDS-sample buffer, and analyzed by Western blotting (loading was normalized to equal cell counts) with VASP- and phospho-VASP–specific antibodies. As control for maximal PKA stimulation, ECV304 cells were treated for 10 min with 10 μM forskolin 72 h after replating. The relative amount of pS157-VASP to total-VASP was quantified from M4 Western blots by densitometric scans (ImageJ version 1.34s; National Institutes of Health).

2D-PAGE proteome analysis of VASP-AAA– and VASP-DDE–binding proteins

Purified recombinant His$_6$-VASP-AAA or -DDE was covalently coupled to Affi-Gel 10 (Bio-Rad Laboratories). Cytosolic proteins from confluent EA.hy926 cells in PBS were prepared as previously described (Herwald et al., 1996) and applied to His$_6$-VASP-AAA or -DDE affinity columns. Columns were washed with PBS, and bound proteins were eluted with glycine/HCl pH 5.0, pH 4.0, pH 3.0, and pH 2.0. pH 2.0 fractions were analyzed by 2D-PAGE and mass spectrometry. Electrophoresis equipment was purchased from GE Healthcare. For first dimension protein separation, protein samples were dissolved in rehydration-buffer (7 M urea, 2 M thiourea, 2% CHAPS, and 2% IPG-buffer 3–10 NL) and applied to IPG strips using the sample cup method. After isoelectric focusing by a standard multistep gradient, strips were equilibrated in buffer E (6 M urea, 2% SDS, 30% glycerine, 50 mM Tris-HCl, 30 mM DTT, and 280 mM iodoacetamide, pH 8.8) and transferred onto 10% Tris-Glycine SDS gels for second dimension protein separation. 2D gels were stained with colloidal Coomassie (G-250), as previously described (Neuhoff et al., 1988), and gel images were processed using the Proteomweaver software version 2.2 (Definiens). Differentially detected spots were excised manually. In some experiments, the SPCN spot migrated as a doublet, probably caused by limited separation capacity of high molecular proteins in the gel system. Gel plugs were washed, equilibrated, and treated with trypsin, as previously described (Shevchenko et al., 1996). Generated peptides were extracted with 0.1% trifluoroacetic acid solution. An aliquot was spotted onto a MALDI-steel target (Bruker Daltonik) together with saturated α-cyano-4-hydroxycinnamic acid solution. MALDI-PMF measurements were performed with an Ultraflex MALDI-TOF/TOF mass spectrometer (Bruker Daltonik). Acquired spectra were processed using the mascot algorithm (V. 1.9) and the current National Center for Biotechnology Information protein database.

Immunoprecipitations and GST pull-down assays

For immunoprecipitation, confluent EA.hy926 cells were lysed (50 mM Tris-HCl, pH 8.0, 500 mM NaCl, 1% NP-40, and protease inhibitor cocktail [Roche]). Lysates were cleared by centrifugation, supernatants were adjusted to 50 mM Tris-HCl, 150 mM NaCl, and 0.3% NP-40, and immunoprecipitated using VASP- and SPCN-specific antibodies or controls. To analyze SPCN-binding to His$_6$-VASP mutants His$_6$-VASP-P177A, -P178A, -P179A, -AAA, and -DAA, we transfected EC-VASP$^{-/-}$ with the constructs, lysed cells 24–36 h later, and immunoprecipitated with αHis$_6$ antibodies. To correlate SPCN–VASP interaction with cell density and VASP phosphorylation, equal numbers of confluent, sparse, and okadaic acid/forskolin–treated (discussed later in this section) confluent ECV304 cells were lysed and immunoprecipitated with αVASP antibodies. To investigate interaction of Cl-VSV and Cl-VSV-SH3 with VASP, ECV304 cells were transiently transfected with the two constructs, lysed 24 h later, and immunoprecipitated with αVASP antibodies. Expression of Cl-VSV did not alter the subcellular VASP distribution as compared with mock-transfected cells. For GST pull-down assays, ECs (EA.hy926, ECV304, EC-VASP$^{+/+}$, EC-VASP$^{-/-}$, and HUVEC) or transfected 293 EBNA cells were grown to confluence and lysed in 40 mM Hepes-NaOH, pH 7.4, 150 mM NaCl, 1% NP-40, and protease inhibitors. Lysates were cleared by centrifugation and incubated with 5 μg immobilized GST-fusion protein or GST alone. GST pull-down assays with purified recombinant VASP were performed as above in this paragraph, using 1 μg PKA-phosphorylated or unphosphorylated His$_6$-VASP or 1 μg of the following mutants: His$_6$-VASP-DDE, -AAA, -DAA, -ADA, -AAE, -P177A, -P178A, and -P179A. Precipitated material was analyzed with anti-His$_6$ antibodies. To analyze whether PKA activity regulates SPCN–VASP interaction in cells, His$_6$-VASP was overexpressed in 293 EBNA cells. 20 h after transfection, cells were either treated with 1 μM okadaic acid (Sigma-Aldrich) and 10 μM forskolin (Sigma-Aldrich) or 10 μM Rp-8-Br-cAMPs (Biolog) for 30 min before cell lysis and GST pull-down experiments.

Endothelial permeability assays

For calcium-switch experiments, ECV304 (or EC-VASP$^{-/-}$) cells were seeded at a density of 7.5×10^4 cells/cm^2 onto PET filters (Becton Dickinson), and 36 h later they were transfected with cDNAs coding for Cl-VSV or Cl-VSV-SH3 (or His$_6$-VASP-WT, -P177A, -P178A, -P179A, -AAA, -DAA, or mock). Transfection rates were determined by FACS analysis using cells that were transfected with a vector coding for enhanced green fluorescent protein. 15 h later, overexpressing cells were washed, incubated in phenol red-free DME (supplemented with 10% FBS and 1.8 mM calcium) and 4 mg/ml FITC-albumin (Sigma-Aldrich) was added to the upper chambers. Basal permeability was followed for 2 h, then extracellular Ca^{2+} was removed by addition of EGTA (4 mM in the apical and the basal chambers; Citi, 1992). 100-μl aliquots were collected from the lower compartments, and FITC-albumin absorbance was measured at 492-nm wavelength (Tecan Spectra Rainbow). Calcium switch experiments with confluent EC-VASP$^{+/+}$ and EC-VASP$^{-/-}$ cells were done accordingly.

Skin vascular leakage assay

5–7-wk-old VASP$^{-/-}$ mice and their wild-type littermates were used. Mice were anesthetized with a single i.p. injection of ketamine/xylazine (80 mg/kg ketamine and 10 mg/kg xylazine), and a total of 200 μl of sterile-filtered 0.25% Evans blue dissolved in sterile saline (0.9% NaCl) was injected i.v. in the retroorbital plexus. 10 min later, 50 μl of bradykinin (100 μM; Sigma-Aldrich) or saline was injected i.d. into the dorsal region by using a tuberculin syringe. The animals were killed 10 min after the

intradermal injections by decapitation. The skin was removed, mounted, and photographed. Skin samples were removed by using a circular template, and the Evans blue dye was extracted by incubating them in *N,N*-dimethyl formamide overnight at 55°C. The next day, the Evans blue fluorescence from individual skin samples was measured at an excitation of 620 nm and an emission of 680 nm.

Online supplemental material

Fig. S1 shows cell–cell contact disassembly and actin reorganization after calcium switch in ECV304 cells. Fig. S2 shows that ECV304 cells do not express detectable levels of endogenous EVL. Fig. S3 shows that profilin does not compete with the SPCN SH3 domain for VASP binding. Table S1 shows primers for the generation of VASP point mutants by site-directed mutagenesis. The online version of this article is available at http://www.jcb.org/cgi/content/full/jcb.200709181/DC1.

We are grateful to Drs. D. Drenckhahn and J. Waschke for generation of EC-VASP$^{+/+}$ and EC-VASP$^{-/-}$, and M. Kuhn for excellent technical support.

This work was supported in part by grants from the Deutsche Forschungsgemeinschaft (DFG) SFB 355 and SFB 688 (to T. Renné). S.M. Feller was supported by Cancer Research UK, and A. Sickmann was supported by DFG FZT 82 and Bundesministerium für Bildung und Forschung Quantpro Project C.

The authors have no conflicting financial interests.

Submitted: 28 September 2007
Accepted: 24 November 2007

Note added in proof. While this paper was in final review, an independent study using genetically altered mice demonstrated increased vascular leakage in Ena/VASP-deficient animals (Furman, C., A.L. Sieminski, A.V. Kwiatkowski, D.A. Rubinson, E. Vasile, R.T. Bronson, R. Fässler, F.B. Gertler. 2007. *J. Cell Biol.* 179:761–775). The study supports the critical role for Ena/VASP-driven actin assembly at endothelial cell–cell junctions in vivo, for which the spectrin–VASP interaction appears to be an important regulator.

References

Ahern-Djamali, S.M., C. Bachmann, P. Hua, S.K. Reddy, A.S. Kastenmeier, U. Walter, and F.M. Hoffmann. 1999. Identification of profilin and src homology 3 domains as binding partners for *Drosophila* enabled. *Proc. Natl. Acad. Sci. USA*. 96:4977–4982.

Bachmann, C., L. Fischer, U. Walter, and M. Reinhard. 1999. The EVH2 domain of the vasodilator-stimulated phosphoprotein mediates tetramerization, F-actin binding, and actin bundle formation. *J. Biol. Chem.* 274:23549–23557.

Ball, L.J., R. Kuhne, B. Hoffmann, A. Hafner, P. Schmieder, R. Volkmer-Engert, M. Hof, M. Wahl, J. Schneider-Mergener, U. Walter, et al. 2000. Dual epitope recognition by the VASP EVH1 domain modulates polyproline ligand specificity and binding affinity. *EMBO J.* 19:4903–4914.

Barzik, M., T.I. Kotova, H.N. Higgs, L. Hazelwood, D. Hanein, F.B. Gertler, and D.A. Schafer. 2005. Ena/VASP proteins enhance actin polymerization in the presence of barbed end capping proteins. *J. Biol. Chem.* 280:28653–28662.

Bear, J.E., T.M. Svitkina, M. Krause, D.A. Schafer, J.J. Loureiro, G.A. Strasser, I.V. Maly, O.Y. Chaga, J.A. Cooper, G.G. Borisy, and F.B. Gertler. 2002. Antagonism between Ena/VASP proteins and actin filament capping regulates fibroblast motility. *Cell.* 109:509–521.

Bennett, V., and A.J. Baines. 2001. Spectrin and ankyrin-based pathways: metazoan inventions for integrating cells into tissues. *Physiol. Rev.* 81:1353–1392.

Blume, C., P.M. Benz, U. Walter, J. Ha, B.E. Kemp, and T. Renne. 2007. AMP-activated protein kinase impairs endothelial actin cytoskeleton assembly by phosphorylating vasodilator-stimulated phosphoprotein. *J. Biol. Chem.* 282:4601–4612.

Bournier, O., Y. Kroviarski, B. Rotter, G. Nicolas, M.C. Lecomte, and D. Dhermy. 2006. Spectrin interacts with EVL (Enabled/vasodilator-stimulated phosphoprotein-like protein), a protein involved in actin polymerization. *Biol. Cell.* 98:279–293.

Brannetti, B., A. Via, G. Cestra, G. Cesareni, and M. Helmer-Citterich. 2000. SH3-SPOT: an algorithm to predict preferred ligands to different members of the SH3 gene family. *J. Mol. Biol.* 298:313–328.

Chen, L., G. Daum, K. Chitaley, S.A. Coats, D.F. Bowen-Pope, M. Eigenthaler, N.R. Thumati, U. Walter, and A.W. Clowes. 2004. Vasodilator-stimulated phosphoprotein regulates proliferation and growth inhibition by nitric oxide in vascular smooth muscle cells. *Arterioscler. Thromb. Vasc. Biol.* 24:1403–1408.

Citi, S. 1992. Protein kinase inhibitors prevent junction dissociation induced by low extracellular calcium in MDCK epithelial cells. *J. Cell Biol.* 117:169–178.

Comerford, K.M., D.W. Lawrence, K. Synnestvedt, B.P. Levi, and S.P. Colgan. 2002. Role of vasodilator-stimulated phosphoprotein in PKA-induced changes in endothelial junctional permeability. *FASEB J.* 16:583–585.

De Matteis, M.A., and J.S. Morrow. 2000. Spectrin tethers and mesh in the biosynthetic pathway. *J. Cell Sci.* 113:2331–2343.

Dejana, E. 2004. Endothelial cell-cell junctions: happy together. *Nat. Rev. Mol. Cell Biol.* 5:261–270.

Drees, B., E. Friederich, J. Fradelizi, D. Louvard, M.C. Beckerle, and R.M. Golsteyn. 2000. Characterization of the interaction between zyxin and members of the Ena/vasodilator-stimulated phosphoprotein family of proteins. *J. Biol. Chem.* 275:22503–22511.

Ermert, L., H. Bruckner, D. Walmrath, F. Grimminger, K. Aktories, N. Suttorp, H.R. Duncker, and W. Seeger. 1995. Role of endothelial cytoskeleton in high-permeability edema due to botulinum C2 toxin in perfused rabbit lungs. *Am. J. Physiol.* 268:L753–L761.

Ferron, F., G. Rebowski, S. Haeng Lee, and R. Dominguez. 2007. Structural basis for the recruitment of profilin–actin complexes during filament elongation by Ena/VASP. *EMBO J.* 26:4597–4606.

Golenhofen, N., W. Ness, E.F. Wawrousek, and D. Drenckhahn. 2002. Expression and induction of the stress protein alpha-B-crystallin in vascular endothelial cells. *Histochem. Cell Biol.* 117:203–209.

Hauser, W., K.P. Knobeloch, M. Eigenthaler, S. Gambaryan, V. Krenn, J. Geiger, M. Glazova, E. Rohde, I. Horak, U. Walter, and M. Zimmer. 1999. Megakaryocyte hyperplasia and enhanced agonist-induced platelet activation in vasodilator-stimulated phosphoprotein knockout mice. *Proc. Natl. Acad. Sci. USA*. 96:8120–8125.

Heltianu, C., I. Bogdan, E. Constantinescu, and M. Simionescu. 1986. Endothelial cells express a spectrin-like cytoskeletal protein. *Circ. Res.* 58:605–610.

Herwald, H., J. Dedio, R. Kellner, M. Loos, and W. Muller-Esterl. 1996. Isolation and characterization of the kininogen-binding protein p33 from endothelial cells. Identity with the gC1q receptor. *J. Biol. Chem.* 271:13040–13047.

Hoffman, L.M., C.C. Jensen, S. Kloeker, C.L. Wang, M. Yoshigi, and M.C. Beckerle. 2006. Genetic ablation of zyxin causes Mena/VASP mislocalization, increased motility, and deficits in actin remodeling. *J. Cell Biol.* 172:771–782.

Howe, A.K., B.P. Hogan, and R.L. Juliano. 2002. Regulation of vasodilator-stimulated phosphoprotein phosphorylation and interaction with Abl by protein kinase A and cell adhesion. *J. Biol. Chem.* 277:38121–38126.

Kang, F., R.O. Laine, M.R. Bubb, F.S. Southwick, and D.L. Purich. 1997. Profilin interacts with the Gly-Pro-Pro-Pro-Pro-Pro sequences of vasodilator-stimulated phosphoprotein (VASP): implications for actin-based Listeria motility. *Biochemistry.* 36:8384–8392.

Kay, B.K., M.P. Williamson, and M. Sudol. 2000. The importance of being proline: the interaction of proline-rich motifs in signaling proteins with their cognate domains. *FASEB J.* 14:231–241.

Krause, M., E.W. Dent, J.E. Bear, J.J. Loureiro, and F.B. Gertler. 2003. Ena/VASP proteins: regulators of the actin cytoskeleton and cell migration. *Annu. Rev. Cell Dev. Biol.* 19:541–564.

Kuhnel, K., T. Jarchau, E. Wolf, I. Schlichting, U. Walter, A. Wittinghofer, and S.V. Strelkov. 2004. The VASP tetramerization domain is a right-handed coiled coil based on a 15-residue repeat. *Proc. Natl. Acad. Sci. USA*. 101:17027–17032.

Kwiatkowski, A.V., F.B. Gertler, and J.J. Loureiro. 2003. Function and regulation of Ena/VASP proteins. *Trends Cell Biol.* 13:386–392.

Lambrechts, A., A.V. Kwiatkowski, L.M. Lanier, J.E. Bear, J. Vandekerckhove, C. Ampe, and F.B. Gertler. 2000. cAMP-dependent protein kinase phosphorylation of EVL, a Mena/VASP relative, regulates its interaction with actin and SH3 domains. *J. Biol. Chem.* 275:36143–36151.

Lawrence, D.W., K.M. Comerford, and S.P. Colgan. 2002. Role of VASP in re-establishment of epithelial tight junction assembly after Ca2+ switch. *Am. J. Physiol. Cell Physiol.* 282:C1235–C1245.

Lawrence, D.W., and K.B. Pryzwansky. 2001. The vasodilator-stimulated phosphoprotein is regulated by cyclic GMP-dependent protein kinase during neutrophil spreading. *J. Immunol.* 166:5550–5556.

Li, S.S. 2005. Specificity and versatility of SH3 and other proline-recognition domains: structural basis and implications for cellular signal transduction. *Biochem. J.* 390:641–653.

Mayer, B.J. 2001. SH3 domains: complexity in moderation. *J. Cell Sci.* 114:1253–1263.

Mehta, D., and A.B. Malik. 2006. Signaling mechanisms regulating endothelial permeability. *Physiol. Rev.* 86:279–367.

Mitic, L.L., and J.M. Anderson. 1998. Molecular architecture of tight junctions. *Annu. Rev. Physiol.* 60:121–142.

Munzel, T., R. Feil, A. Mulsch, S.M. Lohmann, F. Hofmann, and U. Walter. 2003. Physiology and pathophysiology of vascular signaling controlled by guanosine 3′,5′-cyclic monophosphate-dependent protein kinase. *Circulation.* 108:2172–2183.

Neuhoff, V., N. Arold, D. Taube, and W. Ehrhardt. 1988. Improved staining of proteins in polyacrylamide gels including isoelectric focusing gels with clear background at nanogram sensitivity using Coomassie Brilliant Blue G-250 and R-250. *Electrophoresis.* 9:255–262.

Pinder, J.C., and A.J. Baines. 2000. A protein accumulator. *Nature.* 406: 253–254.

Pradhan, D., C.R. Lombardo, S. Roe, D.L. Rimm, and J.S. Morrow. 2001. alpha-Catenin binds directly to spectrin and facilitates spectrin-membrane assembly in vivo. *J. Biol. Chem.* 276:4175–4181.

Price, C.J., and N.P. Brindle. 2000. Vasodilator-stimulated phosphoprotein is involved in stress-fiber and membrane ruffle formation in endothelial cells. *Arterioscler. Thromb. Vasc. Biol.* 20:2051–2056.

Renne, T., K. Schuh, and W. Muller-Esterl. 2005. Local bradykinin formation is controlled by glycosaminoglycans. *J. Immunol.* 175:3377–3385.

Rosenberger, P., J. Khoury, T. Kong, T. Weissmuller, A.M. Robinson, and S.P. Colgan. 2007. Identification of vasodilator-stimulated phosphoprotein (VASP) as an HIF-regulated tissue permeability factor during hypoxia. *FASEB J.* 21:2613–2621.

Rotin, D., D. Bar-Sagi, H. O'Brodovich, J. Merilainen, V.P. Lehto, C.M. Canessa, B.C. Rossier, and G.P. Downey. 1994. An SH3 binding region in the epithelial Na+ channel (alpha rENaC) mediates its localization at the apical membrane. *EMBO J.* 13:4440–4450.

Rotter, B., O. Bournier, G. Nicolas, D. Dhermy, and M.C. Lecomte. 2005. AlphaII-spectrin interacts with Tes and EVL, two actin-binding proteins located at cell contacts. *Biochem. J.* 388:631–638.

Schirenbeck, A., R. Arasada, T. Bretschneider, T.E. Stradal, M. Schleicher, and J. Faix. 2006. The bundling activity of vasodilator-stimulated phosphoprotein is required for filopodium formation. *Proc. Natl. Acad. Sci. USA.* 103:7694–7699.

Schlegel, N., S. Burger, N. Golenhofen, U. Walter, D. Drenckhahn, and J. Waschke. 2007. The role of VASP in the regulation of cAMP- and Rac 1-mediated endothelial barrier stabilization. *Am. J. Physiol. Cell Physiol.* doi:10.1152/ajpcell.00273.2007.

Scott, J.A., A.M. Shewan, N.R. den Elzen, J.J. Loureiro, F.B. Gertler, and A.S. Yap. 2006. Ena/VASP proteins can regulate distinct modes of actin organization at cadherin-adhesive contacts. *Mol. Biol. Cell.* 17:1085–1095.

Sechi, A.S., and J. Wehland. 2004. ENA/VASP proteins: multifunctional regulators of actin cytoskeleton dynamics. *Front. Biosci.* 9:1294–1310.

Shevchenko, A., M. Wilm, O. Vorm, and M. Mann. 1996. Mass spectrometric sequencing of proteins silver-stained polyacrylamide gels. *Anal. Chem.* 68:850–858.

Takahashi, K., Y. Sawasaki, J. Hata, K. Mukai, and T. Goto. 1990. Spontaneous transformation and immortalization of human endothelial cells. *In Vitro Cell. Dev. Biol.* 26:265–274.

Tsukamoto, T., and S.K. Nigam. 1997. Tight junction proteins form large complexes and associate with the cytoskeleton in an ATP depletion model for reversible junction assembly. *J. Biol. Chem.* 272:16133–16139.

Tsukita, S., M. Furuse, and M. Itoh. 2001. Multifunctional strands in tight junctions. *Nat. Rev. Mol. Cell Biol.* 2:285–293.

Vasioukhin, V., C. Bauer, M. Yin, and E. Fuchs. 2000. Directed actin polymerization is the driving force for epithelial cell-cell adhesion. *Cell.* 100:209–219.